Engineering of spin filtering in double epitaxial tunnel junctions

C. Tiusan,[a] F. Greullet, M. Sicot, M. Hehn, C. Bellouard, F. Montaigne , S. Andrieu, and A. Schuhl
Laboratoire de Physique des Matériaux, UMR CNRS 7556, B.P. 239, 54506 Vandœuvre lès Nancy Cedex, France

(Presented on 31 October 2005; published online 19 April 2006)

Double-barrier fully epitaxial crystalline magnetic tunnel junctions employing a class of artificial antiferromagnetic (AAF) subsystem are elaborated by molecular-beam epitaxy. Our specific AAF subsystem is constituted by an Fe(10 nm)/MgO(0.7 nm)/Fe(20 nm) trilayer stack where the antiferromagnetic coupling between the two Fe layers occurs by spin-polarized tunneling of electrons across the three, atomic-layer thin MgO insulating barrier. In our junctions, the efficiency of spin filtering is validated by the tunnel magnetoresistance effects of about 140% at room temperature and a high output voltage up to 500 mV at 1.3 V. © *2006 American Institute of Physics*.
[DOI: 10.1063/1.2166592]

I. INTRODUCTION

Recently, large tunnel magnetoresistance (TMR) effects have been reported[1–4] in MgO crystalline oxide-based magnetic tunnel junctions (MTJs) elaborated either by molecular-beam epitaxy (MBE) or by sputtering. The measured values, above 200%, validate the theoretical predictions[5–7] which explain the large TMR ratios in single-crystalline tunnel junctions by the different tunneling mechanisms and symmetry-related decay rates of the Bloch waves for the majority- and minority-spin channels.

In our group, we have already shown the direct impact of the electronic structure on spin-polarized transport in Fe/MgO/Fe epitaxial magnetic tunnel junctions[8] employing large MgO thickness (2.5–3 nm). We measured giant TMR ratios (100%–170%) at room temperature (RT) in a large class of MgO-based MTJs with different bcc (100) electrodes such as Fe, Co, CoFe, Pd/Fe, and their combination. We have also shown that the interface engineering constitutes a powerful tool to improve the properties for spintronic devices.[9]

On the other hand, for extremely thin insulating barriers, in the equilibrium regime (absence of bias voltage) we pointed out the occurrence of antiferromagnetic (AF) interactions, attributed to the tunneling of electrons.[10] We exploit here this AF coupling to build artificial antiferromagnetic systems, as one of the magnetic subsystems of the MTJs.

In this paper, we present a class of double-barrier epitaxial junctions employing Fe(100) electrodes and MgO insulating layers. One electrode of the junction is a bottom Fe(100)(45 nm) single-crystalline layer. It is separated by a 2.5-nm-thick MgO layer by the other electrode, constituted by the Fe(10 nm)/MgO(0.7 nm)/Fe(20 nm) artificial antiferromagnetic (AAF) system. Typically, the standard AAFs, using Ruderman-Kittel-Kasuya-Yosida (RKKY) interactions across a metallic nonmagnetic spacer, are widely used in MTJ-based devices such as read heads or nonvolatile magnetic random access memories (MRAMs) due to their advantages on the device magnetic properties.[11] Recently, epitaxial Fe/MgO MTJ stacks using standard RKKY-based AAF-type Fe/Cr/Fe have been studied by Przybylski *et al.*[12] The particularity of the AAFs involved in our samples is that the coupling is achieved across an insulating thin MgO spacer (about three monolayers), by quantum tunneling of electrons. Moreover, the epitaxial growth of all the layers ensures the conservation of the crystalline symmetry across all the stack.

II. SAMPLE PREPARATION

The MTJ stacks subjected to our studies were elaborated by molecular-beam epitaxy, in a chamber with a base pressure of 5×10^{-10} Torr. The samples have been grown on (100) MgO substrates, annealed at 600 °C for 20 min. First, a 10-nm-thick seed MgO underlayer was grown at 450 °C. It acts as an antidiffusion barrier which traps the residual C impurities and prevents their diffusion from the substrate within the layers during subsequent annealing stages. Then, the 45-nm-thick Fe bottom electrode is deposited at 100 °C, being subsequently annealed at 450 °C for 20 min to improve its surface quality. The reflection high-energy electron-diffraction (RHEED) patterns illustrated in the top panel of Fig. 1 validate the structural quality of this bottom Fe electrode (denoted Fe-I). Atomic force microscope analysis estimates the surface root-mean-square (rms) roughness after annealing to about 0.1 nm. On the top of the bottom Fe-I layer, a 2.5-nm-thick MgO-I insulating layer was epitaxialy grown by means of an electron gun at RT. A two-dimensional layer-by-layer growth was observed up to five monolayers by means of RHEED intensity oscillations.[13] A second magnetic 10-nm-thick Fe layer was epitaxially grown on the top of the insulating MgO barrier at 100 °C, then subsequently annealed for flattening at 380 °C for 10 min. The structural quality of this Fe-II layer is illustrated in the RHEED patterns shown in the middle panel of Fig. 1. The flatness of this layer is extremely important to ensure the continuity of a three-monolayer thin MgO-II barrier grown on top of the Fe-II. The MgO thickness is precisely monitored using RHEED intensity oscillations,[10] as illustrated in the bottom

[a]Electronic mail: tiusan@lpm.u-nancy.fr

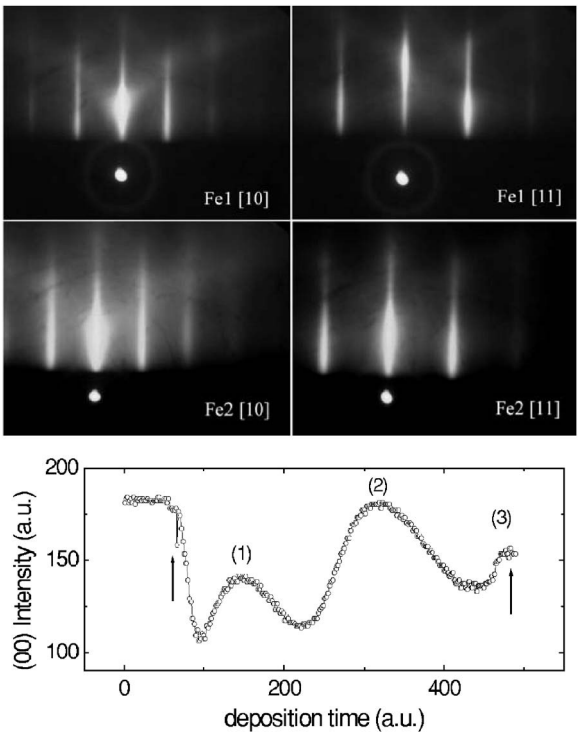

FIG. 1. Top panel: RHEED patterns measured along the [10] and [11] azimuths of the square lattice of the bottom Fe-I. Middle panel: RHEED pattern measured along the [10] and [11] azimuths of the square lattice of the middle Fe-II. Bottom panel: RHEED oscillations observed on the (00) streak during the thin MgO barrier (of the AAF) grown at room temperature. The maxima denoted states 1–3 correspond to the completion of an atomic MgO layer.

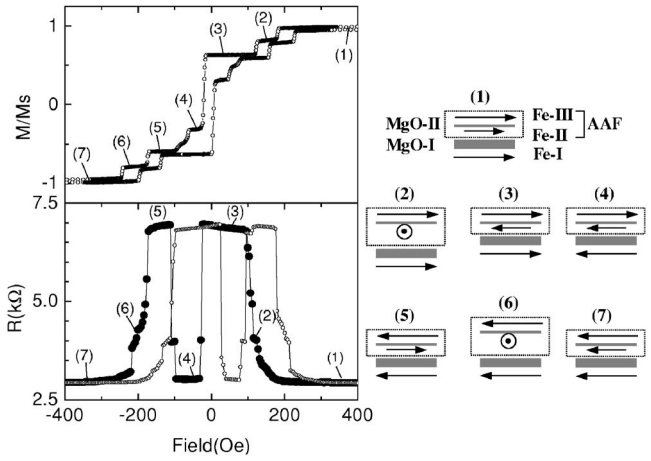

FIG. 2. Top panel: magnetization curve measured on a continuous film Fe(45 nm)/MgO(2.5 nm)/Fe(10 nm)/MgO(0.7 nm)/Fe(20 nm) stack. Bottom panel: resistance vs field curve, measured at 10 mV positive bias, branch from the positive to negative field (-●-) and branch from negative to positive field (-◯-). Right panel: sketch indicating the magnetization configurations in the stack within different field windows from states 1 to 7.

panel of Fig. 1. Last, a 2-nm-thick Fe-III layer is deposited at 100 °C without any annealing. The stack was capped with a Pd(10 nm)/Au(10 nm) protecting bilayer.

After the MBE growth of the multilayer stack, the MTJ structures are patterned by UV lithography and Ar-ion etching, step-by-step controlled *in situ* by Auger spectroscopy.[10]

III. EXPERIMENTAL RESULTS

Let us first consider the magnetic properties of the MTJ stack. The magnetization curve, measured on a continuous film sample prior to lithography, is presented in the top panel of Fig. 2. The field is applied along one of the easy axis of Fe which presents a fourfold anisotropy. The different magnetic configurations are detailed in the right panel sketch.

At the saturation (state 1) all the Fe layers have their magnetization parallel to the field. Reducing the field, the AF coupling tends to stabilize the AF configuration within the AAF. Therefore, during its reversal (state 2), the magnetization of the Fe-II thinner layer of the AAF "flips" to 90° with respect to the field, being "temporarily" trapped by the second, easy-axis-related, anisotropy quantum well of Fe. In the state 3 the AAF is stabilized in the AF configuration, with the net magnetic moment aligned along the positive field. Changing the sign of the field, the bottom Fe-I layer reverses its magnetization (state 4) following the field direction, then the net moment of the AAF switches along the field direction in the state 5. Increasing furthermore the field, the AAF will saturate (state 7) passing again through the intermediate 90° configuration of Fe-II (state 6).

The corresponding tunnel magnetoresistance curve is presented in the bottom panel of Fig. 2. The curve is measured at a bias voltage of 10 mV on a square 10 μm lateral size MTJ with an areal resistance of $2.9\times10^5\ \Omega\ \mu m^2$. The field variation of the resistance validates the magnetic configurations described above in the macroscopic magnetization curve. Indeed, we observe the smallest resistance in state 1 corresponding to the parallel configuration of magnetizations and a maximum of tunnel resistance in state 3 corresponding to the antiparallel configuration. However, in the intermediate states 2 and 6 one does not find exactly half of the resistance variation from states 1 to 3, as expected for a pure 90° configuration of Fe-II indicated in the simplified sketch. This points out the signature of magnetic inhomogeneities within the AAF layers created during the magnetization reversal.[11] Additional investigations by magnetic force microscopy under applied field are in progress.

Having in view the thickness of the two tunnel barriers of the double junction, one can imagine that the voltage drop will mainly take place across the bottom thick MgO-I barrier. Therefore, here the measured resistance reflects the TMR effect of this barrier. However, coherent tunneling events within all the stack should be considered if the thickness of the intermediate Fe-II layer is decreased below 10 nm.[14] These aspects are currently under investigation.

Beyond the amplitude of the tunnel magnetoresistive effect, one of the most important properties of a MTJ for device applications is the variation of the TMR with an external bias voltage. The TMR(V) characteristic is illustrated in Fig. 3(a). As predicted theoretically,[5–7] for large MgO thickness in the asymptotic regime, the tunneling is dominated by a majority *spd*-like character state Δ_1 in the parallel (P) configuration. The propagation of this state in the antiparallel (AP) configuration is "prohibited," which corresponds to a strongly reduced conductivity. In agreement with this frame-

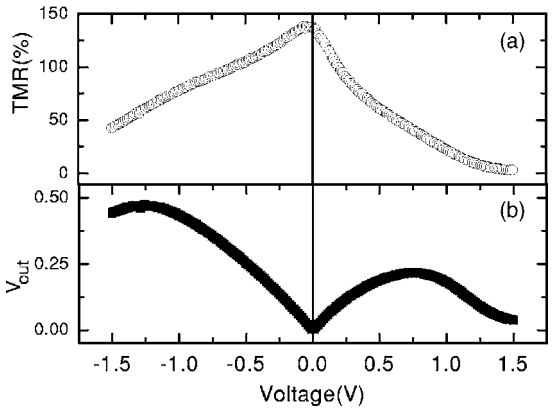

FIG. 3. (a) Magnetoresistance as a function of applied voltage. For each voltage the TMR is calculated as the resistance variation between the saturation (state 1) and the AF plateau (state 3) previously defined in Fig. 2. In positive bias, the positive voltage is applied at the bottom Fe-I electrode. (b) Output voltage vs applied voltage.

work, we measure a large TMR signal of 140% at room temperature. The TMR value decreases with the applied voltage, especially in the low-voltage regime. We associate this behavior to two electronic structure effects: (i) imperfect filtering in the barrier (significant contribution of the Δ_5 symmetry to the tunneling) and (ii) contribution of the interfacial resonance of Fe to the tunneling. A detailed analysis of these two main contributions constitutes the subject of another paper.[9]

For the device applications, the key parameter is the magnitude of the modulation of the output signal, namely, the output voltage defined as $V_{\text{out}}=V(R_{\text{AP}}-R_P)/R_{\text{AP}}$, where V is the applied voltage and R_{AP} and R_P are the junction resistances measured with antiparallel and parallel alignments of the layer magnetizations in contact with the tunnel barrier. From the TMR ratio as a function of the bias voltage, the output voltage for device applications is plotted against the bias voltage, as illustrated in Fig. 3(b). We can see that V_{out} at negative bias voltages can get close to 0.5 V, which is nearly two times that of conventional MTJs with AlO barriers. Similar large values for V_{out} have been reported in standard MgO-based epitaxial MTJs.[2]

IV. CONCLUSION

In conclusion, we elaborate fully epitaxial double-barrier MTJ systems employing artificial antiferromagetic subsystems where the AF interactions are mediated by spin-polarized tunneling of electrons. These junctions present large TMR effects and high output voltage values at large electric bias.

ACKNOWLEDGMENT

The authors acknowledge D. Ligiardi and M. Alnot for technical support.

[1] J. Hayakawa, S. Ikeda, F. Matsukura, H. Takahashi, and H. Ohno, Jpn. J. Appl. Phys., Part 2 **44**, L587 (2005).
[2] S. Yuasa, T. Nagahama, A. Fukushima, Y. Suzuki, and K. Ando, Nat. Mater. **3**, 868 (2004).
[3] D. D. Djayaprawira *et al.*, Appl. Phys. Lett. **86**, 092502 (2005).
[4] S. S. P. Parkin, C. Kaiser, A. Panchula, P. M. Rice, B. Hughes, M. Samant, and S.-H. Yang, Nat. Mater. **3**, 862 (2004).
[5] J. M. MacLaren, X.-G. Zhang, W. H. Buttler, and X. Wang, Phys. Rev. B **59**, 5470 (1999).
[6] W. H. Butler, X.-G. Zhang, T. C. Schulthess, and J. M. MacLaren, Phys. Rev. B **63**, 054416 (2001).
[7] J. Mathon and A. Umerski, Phys. Rev. B **63**, 220403R (2001).
[8] C. Tiusan, J. Faure-Vincent, C. Bellouard, M. Hehn, E. Jouguelet, and A. Schuhl, Phys. Rev. Lett. **93**, 106602 (2004).
[9] C. Tiusan, M. Sicot, J. Faure-Vincent, M. Hehn, C. Bellouard, F. Montaigne, S. Andrieu, and A. Schuhl, J. Phys.: Condens. Matter **18**, 941–956 (2006).
[10] J. Faure-Vincent, C. Tiusan, C. Bellouard, E. Popova, M. Hehn, F. Montaigne, and A. Schuhl, Phys. Rev. Lett. **89**, 107206 (2002).
[11] C. Tiusan, T. Dimopoulos, K. Ounadjela, and M. Hehn, Phys. Rev. B **64**, 104423 (2001), and references therein.
[12] M. Przybylski, J. Grabowski, W. Wulfhekel, M. Rams, K. Tomala, and J. Kirschner, J. Appl. Phys. **95**, 597 (2004).
[13] J. Faure-Vincent *et al.*, Appl. Phys. Lett. **82**, 4507 (2003), and references therein.
[14] The reported coherence length for the majority spin in monocrystalline Fe is above 10 nm, being ten times smaller for the minority spin.